PERGAMON

International Journal of Heat and Mass Transfer 44 (2001) 3321–3333

International Journal of HEAT and MASS TRANSFER

www.elsevier.com/locate/ijhmt

Numerical study of natural convection in an eccentric annulus between a square outer cylinder and a circular inner cylinder using DQ method

C. Shu [a,*], H. Xue [a], Y.D. Zhu [b]

[a] *Department of Mechanical and Production Engineering, National University of Singapore, 10 Kent Ridge Crescent, Singapore 119260*
[b] *Institute of High Performance Computing, 89C Science Park Drive #02-11/12, Singapore 118261*

Received 7 June 2000; received in revised form 12 July 2000

Abstract

In this paper, natural convective heat transfer in a horizontal eccentric annulus between a square outer cylinder and a heated circular inner cylinder is numerically studied using the differential quadrature (DQ) method. The vorticity–stream function formulation is taken in the governing equation. To take the global circulation flow into consideration, the pressure single-value condition is applied, an explicit formulation is derived and the stream function value on the inner cylinder wall is updated from the values at all the interior points. To apply the DQ method, the coordinate transformation is performed. A super elliptic function is introduced in this paper for approximating the square outer boundary located eccentrically to the inner boundary. As a result, the coordinate transformation from the physical domain to the computational domain is set up by an analytical expression. It is demonstrated in this paper that the DQ method is an efficient approach in computing the weak global circulation in the domain. The present method is validated by comparing its numerical results with available data in the literature and very good agreement has been achieved. A systematic study is conducted for the analysis of flow and thermal fields at different eccentricities and angular positions.

1. Introduction

The flow and thermal fields in enclosed space are of great importance due to their wide applications such as in solar collector–receivers, insulation and flooding protection for buried pipes used for district heating and cooling, cooling systems in nuclear reactors, etc. A large number of literature were published in the past few decades. For concentric and eccentric cases in a horizontal annulus between two circular cylinders, the basic and fundamental configuration, the flow and thermal fields have been well studied. Kuehn and Goldstein [1] comprehensively studied the concentric case. The experimental and numerical studies of the eccentric case have been conducted by Kuehn and Goldstein [2], and Guj and Stella [3].

Comparatively, little work has been conducted in more complex domains, such as the annulus between a square outer cylinder and a circular inner cylinder, especially for the eccentric case considered in this paper. For concentric cases, Warrington and Powe [4] reported some experimental results of natural convective heat transfer between concentrically mounted bodies at low Rayleigh numbers. Liu et al. [5] studied the heat convection problem for concentric cases using an operator-splitting pseudo-time-stepping finite element method. Moukalled and Acharya [6] studied numerically natural convective heat transfer from a heated horizontal cylinder placed concentrically inside a square enclosure. The governing equations are solved in a body-fitted coordinate system using a control volume-based numerical procedure. For eccentric cases, Ekundayo et al. [7] studied experimentally the natural convection in horizontal annulus between a square outer cylinder and a circular inner cylinder. Ghaddar [8], and Deschamps and Desrayaud [9] numerically studied the natural convective

* Corresponding author. Fax.: +65-779-1459.
E-mail address: mpeshuc@nus.edu.sg (C. Shu).

0017-9310/01/$ - see front matter
PII: S0017-9310(00)00357-4

Nomenclature

a, b	half length of the axis in the x and y directions for the super elliptic function
a_{ij}, b_{ij}	DQ weighting coefficients of the first- and second-order derivatives
C_p	specific heat at constant pressure
g	gravitational acceleration
h	local heat transfer coefficient
$\bar{h}$	average heat transfer coefficient
k	thermal conductivity
L	side length of the square outer cylinder
n	power of the super elliptic function
$\overline{Nu}$	average Nusselt number
Pr	Prandtl number
r_i	radius of the inner cylinder
r_o	distance from the outer square cylinder to the origin
Ra	Rayleigh number
rr	ratio of L over $2r_i$
x, y	coordinates
T	non-dimensional temperature
u, v	velocity components along x and y directions, respectively
U, V	transformed velocity components along ξ, η directions

Greek symbols

β	thermal expansion coefficient
ξ, η	transformed coordinates
ψ	stream function
ψ_{max}	maximum stream function
ψ_{wall}	stream function on the inner cylinder wall
ω	vorticity
μ	viscosity
ν	kinematic viscosity
ε	eccentricity
φ_o	angular position of outer cylinder

Subscripts

i	values on the inner cylinder wall
o	values on the outer cylinder wall

heat transfer from a uniformly heated horizontal cylinder placed in a large air-filled rectangular enclosure. Sasaguchi et al. [10] numerically studied the effort of the position of a cooled cylinder in a rectangular cavity on the cooling process of water around the cylinder.

In the previous studies for numerical simulation of natural convection in enclosures, low-order methods such as finite difference, finite volume and finite element methods were usually used. In general, the low-order methods need to use a large number of grid points to obtain accurate numerical results, and as a consequence, require large computational effort and virtual storage. On the other hand, the global circulation flow in an eccentric annulus does exist but is very weak, and a high-order method is required in order to obtain an accurate solution. In the present study, the natural convective heat transfer in a horizontal eccentric annulus between a square outer cylinder and a heated circular inner cylinder is numerically studied using the differential quadrature (DQ) method. The vorticity–stream function formulation in the curvilinear co-ordinate system is taken as the governing equation, and the pressure single-value condition is converted to an explicit formulation to update the stream function value on the inner cylinder wall. The SOR iteration method is applied to solve the resultant algebraic equations. The effects of eccentricity and angular position on the flow and thermal fields for the medium aspect ratio are studied in detail.

The DQ method is a global method for numerical discretization. The feature of the DQ method is that it can obtain very accurate numerical results by using a considerably small number of grid points and requires very little computational effort. Like the conventional low-order finite difference schemes, the DQ method also requires the computational domain to be regular. For irregular domain problems such as the one considered in this study, the coordinate transformation technique should be introduced. In this technique, the irregular physical domain is first transformed into a regular computational domain, and the governing equations as well as the boundary conditions are transformed into the relevant forms in the computational space. Then all the computations including the discretization of derivatives by the DQ method are based on the computational space. In this paper, we will demonstrate that the application of the DQ method to irregular domain problems is also very efficient.

For the coordinate transformation, a super elliptic function is introduced in this paper for the square outer boundary located eccentrically to the circular inner cylinder. With the super elliptic function, the coordinate transformation from the physical space to the computational space can be set up by an analytical expression. Thus, all the geometrical parameters can be computed exactly. This simplifies the process of the coordinate transformation.

2. DQ method

The DQ method is a global numerical approach proposed by Bellman et al. [11,12], and greatly im-

proved by Shu and Richards [13,14], and Shu and Chew [15] in the development of explicit formulations for computing the weighting coefficients. For brevity, a one-dimensional problem is chosen in the following to demonstrate the DQ method, where the first- and second-order derivatives of $f(x)$ at a point x_i are approximated by

$$f_x(x_i) = \sum_{j=1}^{N} a_{ij} f(x_j), \quad \text{for } i = 1, 2, \ldots, N, \tag{1}$$

$$f_{xx}(x_i) = \sum_{j=1}^{N} b_{ij} f(x_j), \quad \text{for } i = 1, 2, \cdots, N, \tag{2}$$

where N is the number of grid points, and a_{ij} and b_{ij} are the first- and second-order weighting coefficients, respectively. Obviously, the key procedure in the DQ method is to determine the weighting coefficients a_{ij} and b_{ij}. It was shown by Shu and Richards [13,14], and Shu and Chew [15] that all the ways of computing the weighting coefficients can be generalized under the analyses of function approximation and linear vector space. It was found that when the function $f(x)$ is approximated differently, the formulations for a_{ij} and b_{ij} are also different. In the following, the respective formulations of a_{ij} and b_{ij} are presented when the function $f(x)$ is approximated by a high-order polynomial or by the Fourier series expansion.

2.1. Polynomial-based differential quadrature (PDQ)

In this case, it is supposed that the function is approximated by a $(N-1)$th degree polynomial in the form

$$f(x) = \sum_{k=0}^{N-1} c_k x^k. \tag{3}$$

Under the analysis of a linear vector space, Shu and Richards [13,14], and Shu [16] derived the following explicit formulations for computing the weighting coefficients:

$$a_{ij} = \frac{M^{(1)}(x_i)}{(x_i - x_j) M^{(1)}(x_j)}, \quad \text{when } j \neq i, \tag{4a}$$

$$a_{ii} = -\sum_{k=1, k\neq i}^{N} a_{ik}, \tag{4b}$$

$$b_{ij} = 2a_{ij}\left(a_{ii} - \frac{1}{x_i - x_j}\right), \quad \text{when } j \neq i, \tag{5a}$$

$$b_{ii} = -\sum_{k=1, k\neq i}^{N} b_{ik}, \tag{5b}$$

where

$$M^{(1)}(x_i) = \prod_{k=1, k\neq i}^{N} (x_i - x_k).$$

It is indicated that a recurrence relationship has also been derived to compute the weighting coefficients of the higher-order derivatives. For details, see the work of Shu and Richards [13,14].

2.2. Fourier expansion-based differential quadrature (FDQ)

In this case, the function is approximated by a Fourier series expansion in the form

$$f(x) = c_0 + \sum_{k=1}^{N/2} (c_k \cos kx + d_k \sin kx). \tag{6}$$

Similar to PDQ, Shu and Chew [15], and Shu and Xue [17] also derived the explicit formulations to compute the weighting coefficients a_{ij} and b_{ij}, which are listed below:

$$a_{ij} = \frac{1}{2} \frac{P(x_i)}{\sin((x_i - x_j)/2) P(x_j)}, \quad \text{when } j \neq i, \tag{7a}$$

$$a_{ii} = -\sum_{k=1, k\neq i}^{N} a_{ik}, \tag{7b}$$

$$b_{ij} = a_{ij}\left[2a_{ii} - \cot\frac{x_i - x_j}{2}\right], \quad \text{when } j \neq i, \tag{8a}$$

$$b_{ii} = -\sum_{k=1, k\neq i}^{N} b_{ik}, \tag{8b}$$

where

$$P(x_i) = \prod_{k=0, k\neq i}^{N} \sin\frac{x_i - x_k}{2}.$$

It should be indicated that Eqs. (7a), (7b), (8a) and (8b) can be applied to the periodic problems and the non-periodic problems. For the non-periodic problems, the x range in the computational domain is $0 \leqslant x \leqslant \pi$, while for the periodic problems, the x range in the computational domain is $0 \leqslant x < 2\pi$. For details, refer to the work of Shu and Chew [15].

In the present study, the PDQ and FDQ methods will be used to discretize the spatial derivatives in the governing equations and the boundary conditions. The derivatives in the radial direction are discretized by the PDQ method while the derivatives in the circumferential direction are discretized by the FDQ method.

3. Governing equations and boundary conditions

A schematic view of a horizontal eccentric annulus between a square outer cylinder and a heated circular

inner cylinder is shown in Fig. 1. Heat is generated uniformly within the circular inner cylinder, which is placed eccentrically within the cold square cylinder. The imposed boundary conditions are no-slip and isothermal walls on both cylinders.

Based on the Boussinesq approximation, the non-dimensional governing equation for the problem is written in the vorticity–stream function formulation as

$$\frac{\partial^2\psi}{\partial x^2}+\frac{\partial^2\psi}{\partial y^2}=\omega, \tag{9}$$

$$u\frac{\partial\omega}{\partial x}+v\frac{\partial\omega}{\partial y}=Pr\left(\frac{\partial^2\omega}{\partial x^2}+\frac{\partial^2\omega}{\partial y^2}\right)-PrRa\frac{\partial T}{\partial x}, \tag{10}$$

$$u\frac{\partial T}{\partial x}+v\frac{\partial T}{\partial y}=\frac{\partial^2 T}{\partial x^2}+\frac{\partial^2 T}{\partial y^2}, \tag{11}$$

where ψ denotes stream function, ω represents vorticity, and T is the temperature. Prandtl number is defined as $Pr=\mu C_p/k$, and Rayleigh number is defined as $Ra=(C_p\rho_0 g\beta L^3\Delta T)/kv$. Here μ is the viscosity, C_p the specific heat at constant pressure, k the thermal conductivity, ρ_0 the reference density, g the gravitational acceleration, β the thermal expansion coefficient, L the side length of the square outer cylinder, ΔT the temperature difference between inner and outer cylinders, and v is the kinematic viscosity. Velocity components u and v can be computed from the stream function ψ as

$$u=\frac{\partial\psi}{\partial y},\quad v=-\frac{\partial\psi}{\partial x}. \tag{12}$$

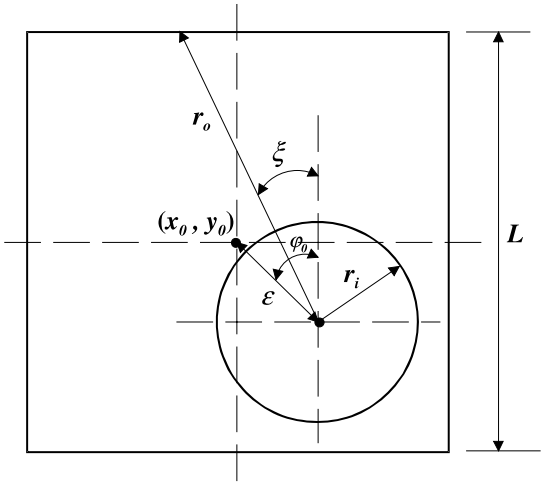

Fig. 1. Sketch of physical domain.

Using the expressions in Eq. (12), Eq. (9) can also be written as

$$\omega=\frac{\partial u}{\partial y}-\frac{\partial v}{\partial x}. \tag{13}$$

Like the low-order finite difference schemes, the DQ method requires the physical boundary to be a mesh line. In the present study, however, the physical boundaries may not coincide with the mesh lines. When the DQ method is applied to this case, the physical boundary conditions cannot be implemented in a straightforward way. To overcome this difficulty, the following transformation from the physical space to the computational space is required:

$$\begin{cases}\xi=\xi(x,y)\\ \eta=\eta(x,y).\end{cases} \tag{14}$$

With this transformation, the governing equations (9)–(11) can be transformed to the following forms in the computational space:

$$A\frac{\partial^2\psi}{\partial\xi^2}+2B\frac{\partial^2\psi}{\partial\eta\partial\xi}+C\frac{\partial^2\psi}{\partial\eta^2}+G\frac{\partial\psi}{\partial\eta}+H\frac{\partial\psi}{\partial\xi}=J\omega, \tag{15}$$

$$\begin{aligned}U\frac{\partial\omega}{\partial\xi}+V\frac{\partial\omega}{\partial\eta}&=Pr\left(A\frac{\partial^2\omega}{\partial\xi^2}+2B\frac{\partial^2\omega}{\partial\xi\partial\eta}+C\frac{\partial^2\omega}{\partial\eta^2}+G\frac{\partial\omega}{\partial\eta}+H\frac{\partial\omega}{\partial\xi}\right)\\&\quad-PrRa\left(y_\eta\frac{\partial T}{\partial\xi}-y_\xi\frac{\partial T}{\partial\eta}\right),\end{aligned} \tag{16}$$

$$U\frac{\partial T}{\partial\xi}+V\frac{\partial T}{\partial\eta}=\left(A\frac{\partial^2 T}{\partial\xi^2}+2B\frac{\partial^2 T}{\partial\xi\partial\eta}+C\frac{\partial^2 T}{\partial\eta^2}+G\frac{\partial T}{\partial\eta}+H\frac{\partial T}{\partial\xi}\right), \tag{17}$$

where

$$\begin{aligned}&U=\frac{\partial\psi}{\partial\eta},\quad V=-\frac{\partial\psi}{\partial\xi},\quad A=\alpha/J,\quad B=-\sigma/J,\\&C=\gamma/J,\quad G=\frac{\partial B}{\partial\xi}+\frac{\partial C}{\partial\eta},\quad H=\frac{\partial A}{\partial\xi}+\frac{\partial D}{\partial\eta},\\&\alpha=x_\eta^2+y_\eta^2,\quad \sigma=x_\xi x_\eta+y_\xi y_\eta,\quad \gamma=x_\xi^2+y_\xi^2,\\&J=x_\xi y_\eta-y_\xi x_\eta,\end{aligned} \tag{18}$$

where x_ξ, x_η, y_ξ and y_η are respectively the abbreviations of $\partial x/\partial\xi$, $\partial x/\partial\eta$, $\partial y/\partial\xi$ and $\partial y/\partial\eta$.

From the no-slip condition, the velocities U and V on both the inner and outer cylinder walls are zero. For an eccentric annulus, the stream function values on the inner and outer cylinders are different and a global circulation flow along the inner cylinder exists. The stream function value on the outer cylinder wall is set to zero in the present study. The boundary conditions can be written as

$$U\Big|_{\eta=0,1}=0,\quad V\Big|_{\eta=0,1}=0 \tag{18a}$$

$$\psi\Big|_{\eta=0}=\text{constant},\quad \psi\Big|_{\eta=1}=0 \tag{18b}$$

$$T\Big|_{\eta=0}=1,\quad T\Big|_{\eta=1}=0 \tag{18c}$$

The boundary condition for vorticity ω can be derived from Eq. (15)

$$\omega\Big|_{\eta=0,1}=\frac{C}{J}\frac{\partial^2\psi}{\partial\eta^2}\Big|_{\eta=0,1}=\frac{C}{J}\frac{\partial U}{\partial\eta}\Big|_{\eta=0,1}. \tag{19}$$

Furthermore, Neumann boundary condition for the stream function can be derived from Eq. (18a) as

$$\frac{\partial\psi}{\partial\eta}\Big|_{\eta=0,1}=0. \tag{20}$$

The periodic condition in the ξ direction is automatically implemented by FDQ method.

4. Super elliptic function and analytical coordinate transformation

As shown in Fig. 1, the physical domain is formed by a square outer cylinder and a circular inner cylinder. The DQ method cannot be directly applied to solve this problem in both the Cartesian coordinate system and the cylindrical coordinate system. To apply the DQ method, we have to perform the coordinate transformation, which maps the physical domain to a rectangular domain in the computational space. Usually, the coordinate transformation is made by numerical grid generation technique. In this technique, the geometrical parameters such as x_ξ, x_η, y_ξ and y_η are approximated by a numerical discretization technique. Obviously, this treatment will introduce additional numerical errors into the computation, which may have some effects on the accuracy of numerical results. As will be shown below, a super elliptic function can be used to accurately approximate a rectangular boundary. So, for the problem considered in this study, an analytical expression can be derived for the coordinate transformation from the physical space to the computational space. Then all the geometrical parameters can be computed exactly. The super elliptic function can be written as

$$\left(\frac{x-x_0}{a}\right)^{2n}+\left(\frac{y-y_0}{b}\right)^{2n}=1, \tag{21}$$

where n is a positive integer, a and b half of the elliptic lengths in the x and y directions, respectively, and x_0 and y_0 are the coordinates at the center of square outer cylinder. When $x_0=0$ and $y_0=0$, the problem is a concentric case. When $x_0\neq 0$ and $y_0\neq 0$, the considered problem is an eccentric case. It is interesting to see that when $n=1$ and $a\neq b$, the geometry represented by Eq. (21) is an ellipse; and when $n=1$ and $a=b$, the geometry becomes a circle. As n increases from 1, the geometry would approach a rectangle for $a\neq b$ or a square for $a=b$. The geometries varying with n for $a=b$ are shown in Fig. 2. It can be concluded that when n is above 20, the geometry keeps very little change with the increase of n and remains in a square with tiny round corner. Therefore the non-dimensional square outer cylinder in an eccentric position can be approximated by

$$(x-x_0)^{2n}+(y-y_0)^{2n}=1 \tag{22}$$

with the use of a large value of n.

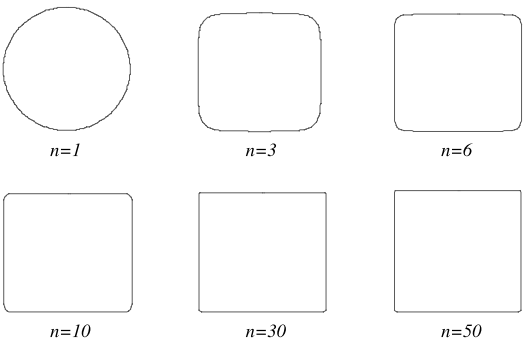

Fig. 2. Effect of power n on geometry.

With Eq. (22), the coordinate transformation for the present problem can be exactly set up, which is written as

$$x=-\sin\xi[r_i+(r_o-r_i)\eta], \tag{23a}$$

$$y=\cos\xi[r_i+(r_o-r_i)\eta], \tag{23b}$$

where r_i is the radius of the inner cylinder, which is a constant, and r_o is derived from Eq. (22) as

$$r_o=\frac{b}{\left[\left(\frac{b}{a}\right)^{2n}\left(\sin\xi+\frac{x_0}{r_0}\right)^{2n}+\left(\cos\xi-\frac{y_0}{r_0}\right)^{2n}\right]^{1/2n}}, \tag{24}$$

where r_o can be computed by iteration. The transformed computational domain in the $(\xi,\ \eta)$ plane is $0\leqslant\eta\leqslant 1$ and $0\leqslant\xi\leqslant 2\pi$. With Eqs. (23a), (23b) and (24), the parameters A, B, C, G, H, α, σ, γ, J used in Eqs. (15)–(17) can be computed accurately.

5. Pressure single-value condition and computation of stream function value on inner cylinder wall

As mentioned in the previous section, the global circulation flow does exist but is very weak in the flow field. The pressure single-value condition is required to update the stream function value on the inner cylinder wall.

According to the pressure single-value condition, we have $\oint_l \nabla p\,\mathrm{d}\bar{l}=0$, where $\bar{l}$ can be taken as the inner

cylinder boundary along anti-clockwise direction. Along the inner cylinder boundary in the computational domain, we have

$$\int_0^{2\pi} \frac{\partial p}{\partial \xi} \mathrm{d}\xi = 0. \tag{25}$$

The expression of $\partial p/\partial \xi$ on the inner cylinder wall can be derived from the momentum equation, which is written as

$$\left.\frac{\partial p}{\partial \xi}\right|_{\eta=0} = -\frac{r_\mathrm{i}}{(r_\mathrm{o}-r_\mathrm{i})^3}\frac{\partial^3 \psi}{\partial \eta^3} - \frac{1}{(r_\mathrm{o}-r_\mathrm{i})^2}\frac{\partial^2 \psi}{\partial \eta^2} - r_\mathrm{i} PrRaT \sin\xi. \tag{26}$$

The derivatives in Eq. (26) can be discretized by the PDQ method. With Eqs. (18b), (20) and (26), Eq. (25) can be simplified to give

$$\psi_\mathrm{wall} = -\frac{\int_0^{2\pi}(\mathrm{SUM3}+\mathrm{SUM2})\mathrm{d}\xi}{q_1 I + p_1 \bar{I}}, \tag{27}$$

where

$$\begin{aligned}
\mathrm{SUM3} &= \frac{r_\mathrm{i}}{(r_\mathrm{o}-r_\mathrm{i})^3}\sum_{k=3}^{M-2} q_k \psi_{i,k},\\
\mathrm{SUM2} &= \frac{1}{(r_\mathrm{o}-r_\mathrm{i})^2}\sum_{k=3}^{M-2} p_k \psi_{i,k},\\
I &= \int_0^{2\pi} \frac{r_\mathrm{i}}{(r_\mathrm{o}-r_\mathrm{i})^3}\mathrm{d}\xi,\\
\bar{I} &= \int_0^{2\pi} \frac{1}{(r_\mathrm{o}-r_\mathrm{i})^2}\mathrm{d}\xi,\\
p_k &= \bar{b}_{1,k} + \bar{b}_{1,M-1}\bar{q}_k - \bar{b}_{1,2}\bar{p}_k,\\
q_k &= \bar{c}_{1,k} + \bar{c}_{1,M-1}\bar{q}_k - \bar{c}_{1,2}\bar{p}_k,\\
\bar{p}_k &= \left(\bar{a}_{1,k}\bar{a}_{M,M-1} - \bar{a}_{M,k}\bar{a}_{1,M-1}\right)/\Delta,\\
\bar{q}_k &= \left(\bar{a}_{1,k}\bar{a}_{M,2} - \bar{a}_{M,k}\bar{a}_{1,2}\right)/\Delta,\\
\Delta &= \bar{a}_{1,2}\bar{a}_{M,M-1} - \bar{a}_{M,2}\bar{a}_{1,M-1}.
\end{aligned} \tag{28}$$

$\bar{a}_{1,k}$, $\bar{b}_{1,k}$ and $\bar{c}_{1,k}$ are respectively the weighting coefficients of the first-, second- and third-order derivatives in the η direction. Note that p_1, q_1, I and $\bar{I}$ can be computed once and stored for all the following computations. Eq. (27) indicates that the stream function on the inner cylinder wall can be updated by the stream function values at the interior points, which are computed from the governing equations.

6. Results and discussion

In the present study, Rayleigh number is fixed at 3×10^5 in a steady laminar boundary-layer regime, and Prandtl number is set to be 0.71. The numerical investigation is conducted for different eccentricities and angular positions of the outer cylinder. The power n used in the super elliptic function is taken to be 50 for a good approximation of the square boundary. The PDQ method is applied in the η direction with non-uniform grid point distribution, while the FDQ method is applied in the ξ direction with uniform grid point distribution. The grid point distributions are taken as

$$\xi_i = \frac{i-1}{N}2\pi, \quad \eta_j = \frac{1}{2}\left[1-\cos\left(\frac{j-1}{M-1}\pi\right)\right], \quad i=1,2,\ldots,N;\ j=1,2,\ldots,M. \tag{29}$$

After numerical discretization by the DQ method, the resultant algebraic equations are solved by the SOR iteration method. In the present study, the initial values are set to zero for ψ, u, v, T and ω at the interior points. The Nusselt numbers are defined in the same way as shown in the work of Moukalled and Acharya [6].

6.1. Definition of Nusselt numbers

The local heat transfer coefficient h is expressed as

$$h = -k\frac{\partial T}{\partial n}, \tag{30}$$

where k is the thermal conductivity. The average heat transfer coefficient $\bar{h}$ can be computed as

$$\bar{h} = \frac{1}{2\pi}\int_0^{2\pi} h\,\mathrm{d}\xi. \tag{31}$$

The average Nusselt numbers for the inner and the outer boundaries are respectively determined by

$$\overline{Nu}_\mathrm{i} = \frac{\bar{h}_\mathrm{i} S_\mathrm{i}}{k}, \quad \overline{Nu}_\mathrm{o} = \frac{\bar{h}_\mathrm{o} S_\mathrm{o}}{k}, \tag{32}$$

where S_i and S_o are defined in the same way as in the work of Moukalled and Acharya [6]. In their work, the computational domain is taken as half of the physical domain due to the symmetry, so S_i and S_o are taken as half of the circumferential lengths of the inner and outer cylinder surfaces, respectively. Since at steady state, the Nusselt numbers along the inner and outer walls are the same, there is no need to pay separate attention to $\overline{Nu}_\mathrm{i}$ and $\overline{Nu}_\mathrm{o}$. Thus in this study, we only show the value of $\overline{Nu}_\mathrm{i}$, which is also noted as $\overline{Nu}$.

6.2. Grid-independent study

The grid independence of numerical results is studied for the case of $Ra = 3\times10^5$, $rr = L/(2r_\mathrm{i}) = 2.6$, $Pr = 0.71$, $\varepsilon = 0.50$ and $\varphi_0 = 0°$. The numerical results using five different mesh sizes are shown in Table 1. It can be seen from the table that when the mesh size is above 31×21, the computed ψ_max and $\overline{Nu}$ remain the same. Thus, we can say that the mesh size of 31×21 is

Table 1
Grid independence study for $Ra = 3 \times 10^5$, $Pr = 0.71$, $rr = 2.6$, $\varphi_0 = 0°$ and $\varepsilon = 0.50$

Item	Grid point	$\overline{Nu}$	ψ_{max}
1	25×15	7.10	21.72
2	31×17	6.99	21.43
3	31×19	6.98	21.40
4	31×21	6.98	21.43
5	31×23	6.98	21.43

fine enough to give accurate numerical results for the case of $Ra = 3 \times 10^5$. It is also shown in Table 1 that the DQ method only requires very few grid points to obtain accurate numerical results.

The minimum mesh size for a grid-independent solution depends on the complexity of the flow and thermal fields, eccentricity and the angular position. When Rayleigh number is fixed at 3×10^5, the minimum mesh size mainly depends on the eccentricity and the angular position. From our numerical experiments, it was found that for small eccentricity $\varepsilon = 0.25$ and $\varepsilon = 0.50$ at all angular positions, 31×21 and 41×21 grid points are adequate to yield accurate results. When the eccentricity increases and the angular position changes, more grid points should be used to obtain accurate results. In this study, the mesh sizes of 31×21, 41×21, 49×39 and 59×49 are used, respectively, for different combinations of eccentricities and angular positions.

6.3. Effect of power n on numerical results

The effect of power n of the super elliptic function on the approximation of the geometry has been studied in the previous section, and some results are displayed in Fig. 2. In this section, we will study the effect of power n on the numerical results. Table 2 lists the change of $\overline{Nu}$ and ψ_{max} with power n for the case of $Ra = 3 \times 10^5$, $Pr = 0.71$, $rr = 2.6$, $\varphi_0 = 0°$ and $\varepsilon = 0.50$. It is clearly shown in the table that $\overline{Nu}$ and ψ_{max} remain the same when the power n exceeds 10 and 20, respectively. For accurate numerical results and good geometry approximation, the power n is taken to be 50 in the following study.

Table 2
Effect of power n on numerical results for $Ra = 3 \times 10^5$, $Pr = 0.71$, $rr = 2.6$, $\varphi_0 = 0°$ and $\varepsilon = 0.50$

Item	n	$\overline{Nu}$	ψ_{max}
1	1	6.75	17.21
2	3	6.95	21.44
3	6	6.97	21.57
4	10	6.98	21.48
5	20	6.98	21.43
6	30	6.98	21.43
7	40	6.98	21.43
8	50	6.98	21.43

6.4. Validation of numerical results

As discussed in the introduction, most research work focused on the study of natural convection in annuli between either concentric or eccentric circular cylinders. Only a few publications were involved in an annulus between a square outer cylinder and a circular inner cylinder. In the work of Moukalled and Acharya [6], three different aspect ratios and four different Rayleigh numbers were considered. The governing equations were solved in a body-fitted coordinate system using a control volume-based numerical procedure. Their numerical data were validated by comparison with some experimental data and found in good agreement. In the work of Liu et al. [5], the circular inner cylinder was concentrically located inside a rectangular cylinder and only one aspect ratio was considered at two different Rayleigh numbers. The problem was solved by an operator-splitting pseudo-time-stepping finite element method. Thus, in this study, the results of Moukalled and Acharya [6] are used to validate the present numerical results. The maximum stream function value ψ_{max} and the average Nusselt number $\overline{Nu}$ between the present work and the work of Moukalled and Acharya [6] are compared in Table 3 for Rayleigh numbers of 10^4, 10^5, 10^6 and aspect ratios of 5.0, 2.5 and 1.67. It should be noted that due to the different ways of non-dimensionalization between the work of Moukalled and Acharya [6] and the present study, the equivalent ψ_{max} in Table 3 is the one given from Moukalled and Acharya [6] multiplying by the Prandtl number. From Table 3, it can be seen that the present results generally agree well with those of Moukalled and Acharya [6].

6.5. Global circulation

The angular directions of 0° and 180° are two special cases in the eccentric annulus. It can be seen from Figs. 3 and 4 that the flow and thermal fields are symmetric about the vertical line connecting the centers of both cylinders. The inner cylinder is always surrounded by a thermal boundary layer while the presence of a boundary layer on the outer cylinder depends on the inner cylinder position. When the inner cylinder is near the bottom of the cavity, the stagnant area reduces to its minimum. When the inner cylinder is moved near the top, there is no boundary layer on the bottom portion of the outer cylinder. Two eddies are found to be symmetric in the physical domain. The flow and thermal fields are symmetrical. The global circulation does not exist at different eccentricities in these two cases.

For other angular positions, global circulation flow occurs for all eccentricities. This can be observed in

Table 3
Comparison of ψ_{max} and $\overline{Nu}$ ($Pr = 0.71$)

$rr = \frac{L}{2r_i}$	Ra	ψ_{max}		$\overline{Nu}$	
		Present	Moukalled et al. [6] (equivalent)	Present	Moukalled et al. [6]
5.0	10^4	1.71	1.73	2.082	2.071
2.5		0.97	1.02	3.245	3.331
1.67		0.49	0.50	5.395	5.826
5.0	10^5	9.93	10.15	3.786	3.825
2.5		8.10	8.38	4.861	5.080
1.67		5.10	5.10	6.214	6.212
5.0	10^6	20.98	25.35	6.106	6.107
2.5		24.13	24.07	8.898	9.374
1.67		20.46	21.30	12.000	11.620

Table 4, which shows the stream function value on the inner cylinder wall, ψ_{wall}. It is noted that when the global circulation flow is occurred, ψ_{wall} is not zero. The formation of global circulation flow is probably due to unbalance of the buoyant forces in the left and right sides of the vertical centerline.

6.6. Analysis of flow and thermal fields

Analysis of flow and thermal fields is made at different angular position φ_0. The computational results of ψ_{max}, ψ_{wall} and $\overline{Nu}$ are listed in Table 4. The streamlines and isotherms are shown in Figs. 3–7 for different angular positions.

Table 4
Results in the arbitrary eccentric annuli for $Ra = 3\times 10^5$, $Pr = 0.71$, $rr = 2.6$

φ_0	ε	ψ_{max}	ψ_{wall}	$\overline{Nu}$
	0.00	15.63	$<10^{-4}$	6.52
0°	0.25	18.67	$<10^{-4}$	6.75
	0.50	21.43	$<10^{-4}$	6.98
	0.75	24.07	$<10^{-4}$	7.95
	0.95	24.57	$<10^{-4}$	11.71
45°	0.25	18.84	0.11	6.90
	0.50	19.75	0.47	6.92
	0.75	20.65	1.46	7.06
	0.95	21.68	1.80	7.61
90°	0.25	17.15	−0.15	6.73
	0.50	18.77	1.64	6.72
	0.75	16.83	1.05	7.40
	0.95	16.51	0.03	11.15
135°	0.25	15.56	0.12	6.48
	0.50	14.60	0.84	6.25
	0.75	13.94	1.25	6.23
	0.95	12.96	0.93	6.45
180°	0.25	12.55	$<10^{-4}$	7.05
	0.50	11.32	$<10^{-4}$	6.17
	0.75	10.26	$<10^{-4}$	6.90
	0.95	9.19	$<10^{-4}$	10.58

For $\varphi_0 = 0°$ as shown in Fig. 3, the flow and thermal fields are symmetric. The flow fields show explicitly that the two centers of the two symmetric eddies on the left-hand side (LHS) and right-hand side (RHS) move closer with eccentricity. This is because the great space is then available for circulation to occur when the eccentricity increases, and the two eddies increase their sizes towards the center of the square outer cylinder. The maximum value of the stream function increases from 15.63 for the concentric case to 24.57 for $\varepsilon = 0.95$ (Table 4). The stagnant area under the inner cylinder decreases with increase of eccentricity but still exists at the two bottom corners of the square cylinder. A large plume exists in the large gap above the inner cylinder, which creates a thinner thermal boundary layer on top of the square cylinder.

For $\varphi_0 = 180°$ as shown in Fig. 4, the flow and thermal fields are symmetric. The maximum value of stream function decreases with eccentricity considerably, from 15.63 for the concentric case to 9.19 for $\varepsilon = 0.95$ (Table 4). For $\varepsilon = 0.25$, two additional eddies are found above the inner cylinder. Two plumes appear on top of the inner cylinder with about 40° from the vertical centerline, and a third plume appears above top of the inner cylinder with reverse direction. The two additional eddies on top of the inner cylinder cause the formation of the third plume to appear in the reverse direction. For the case of $\varepsilon = 0.75$, the two additional eddies disappear and the two plumes become weak. The third plume that occurs in the reverse direction disappears. This is probably due to the fact that the increased eccentricity reduces the space above the top of the inner cylinder and some heat conduction occurs on top of the inner cylinder. The average Nusselt number increases slightly from 6.52 for the concentric case to 7.05 for the case of $\varepsilon = 0.25$, then decreases slightly to the minimum 6.17 at $\varepsilon = 0.50$. It increases again to reach 6.90 for the case of

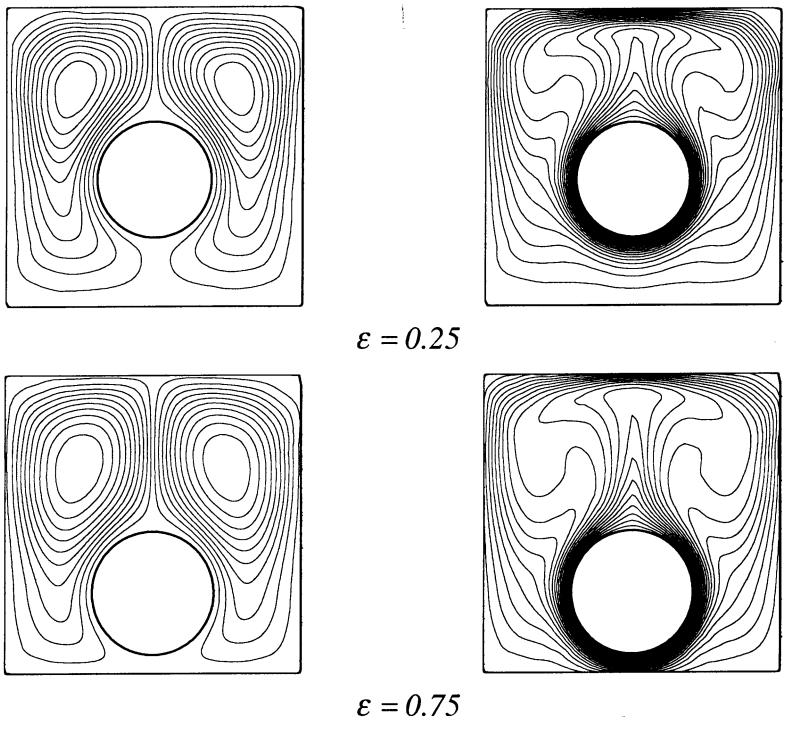

Fig. 3. Streamlines and isotherms for $Ra = 3 \times 10^5$, $Pr = 0.71$, $rr = 2.6$, $\varphi_0 = 0°$.

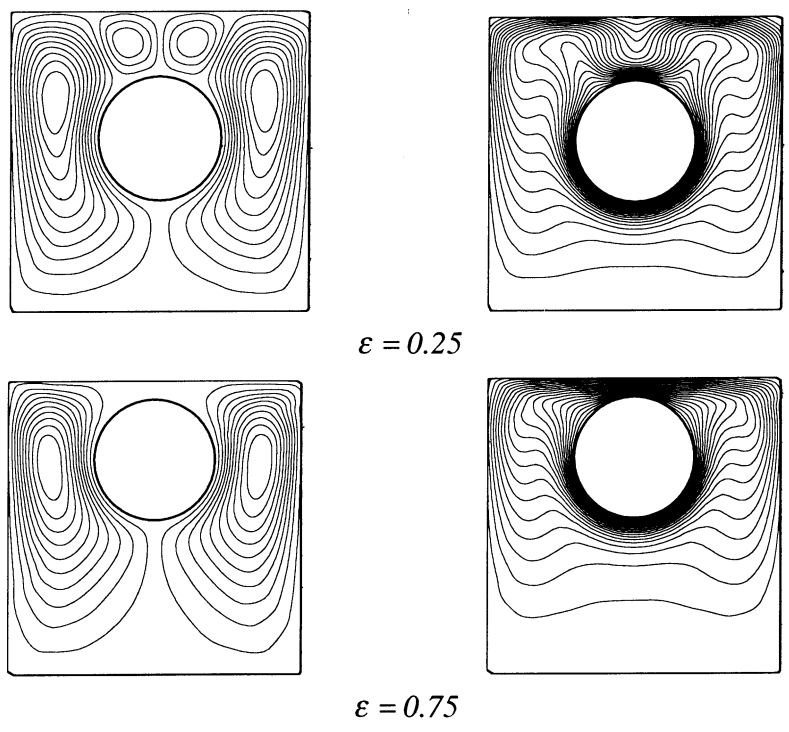

Fig. 4. Streamlines and isotherms for $Ra = 3 \times 10^5$, $Pr = 0.71$, $rr = 2.6$, $\varphi_0 = 180°$.

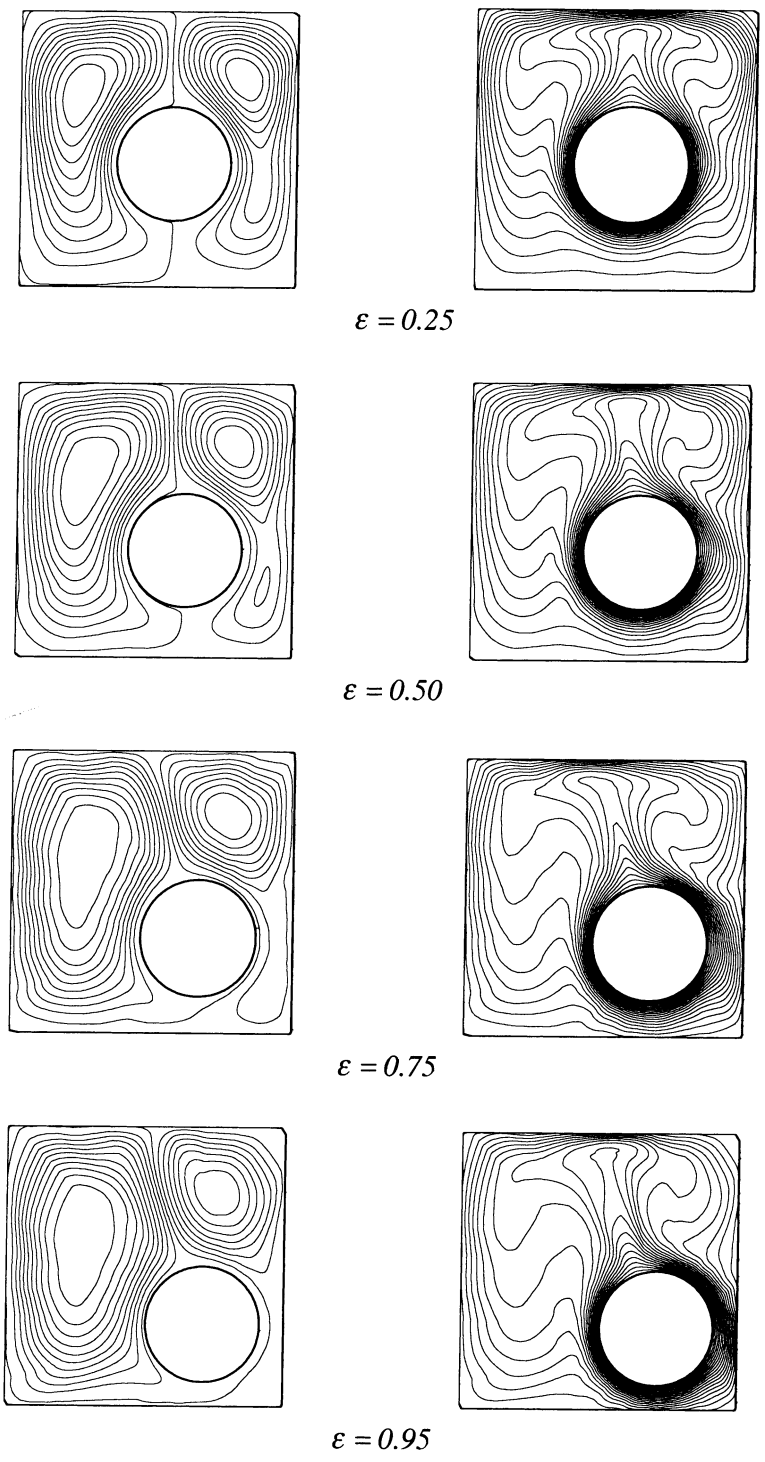

Fig. 5. Streamlines and isotherms for $Ra = 3 \times 10^5$, $Pr = 0.71$, $rr = 2.6$, $\varphi_0 = 45°$.

$\varepsilon = 0.75$, and then increases substantially for the case of $\varepsilon = 0.95$. A large portion of stagnant area increases with the eccentricity.

For $\varphi_0 = 45°$ as shown in Fig. 5, the eddy on the LHS in the flow expands in size due to the increasing space, with the center of the eddy moving downwards.

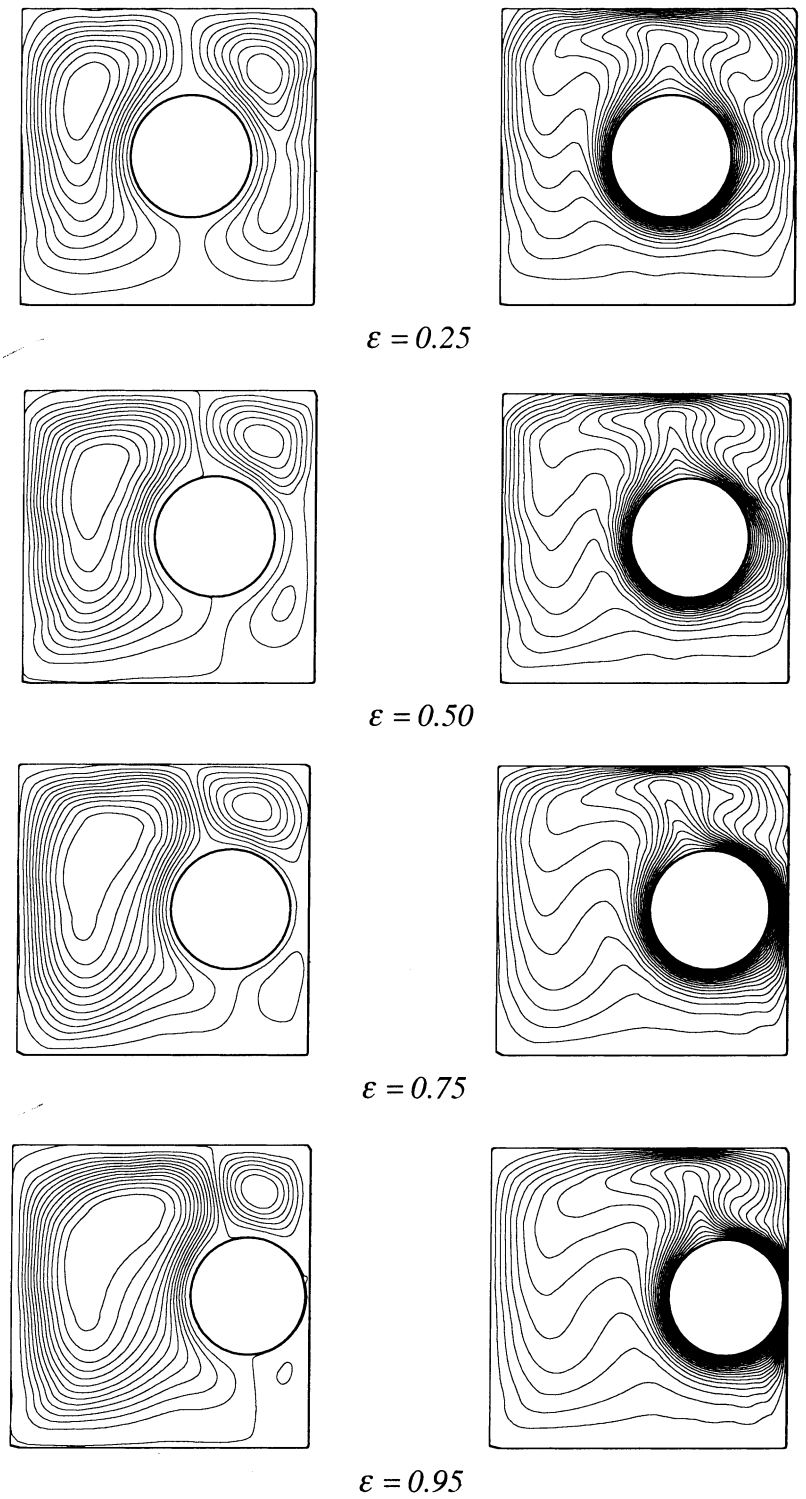

Fig. 6. Streamlines and isotherms for $Ra = 3 \times 10^5$, $Pr = 0.71$, $rr = 2.6$, $\varphi_0 = 90°$.

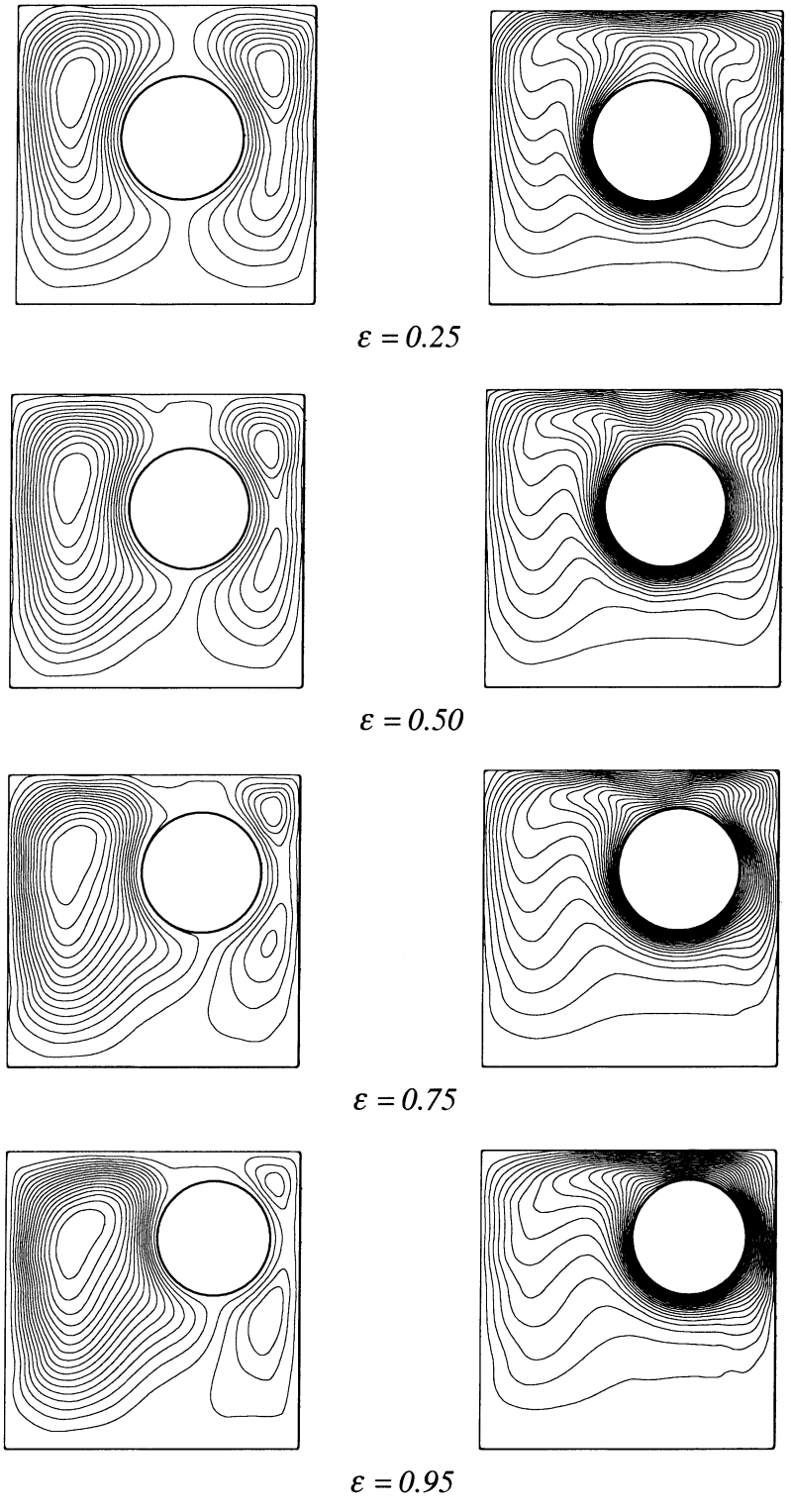

Fig. 7. Streamlines and isotherms for $Ra = 3 \times 10^5$, $Pr = 0.71$, $rr = 2.6$, $\varphi_0 = 135°$.

The eddy on the RHS remains the similar size but shifts above the inner cylinder. The increasing eccentricity allows larger space for the eddy on the RHS, but the increasing eddy on the LHS limits the space for the eddy on the RHS. The maximum value of stream function increases from 15.63 for the concentric case to 21.68 for the case of $\varepsilon = 0.95$. The plume above the top of the inner cylinder shifts from the vertical line to the left. The average Nusselt number remains almost unchanged except for the case of $\varepsilon = 0.95$. The stagnant area decreases with eccentricity.

For $\varphi_0 = 90°$ as shown in Fig. 6, the eddy on the LHS in the flow expands in size due to the increasing space. The eddy on the RHS separates into two small eddies, above and below the inner cylinder respectively, with the increasing eccentricity. The maximum values of stream function are about the same level at different eccentricity, but the average Nusselt number increases greatly for the case of $\varepsilon = 0.95$, where the inner cylinder is very close to the wall of the outer cylinder.

For $\varphi_0 = 135°$ as shown in Fig. 7, the eddy on the RHS finally separates into two with eccentricity due to the reduced space. The maximum value of stream function decreases slightly from 15.63 for the concentric case to 12.96 for the case of $\varepsilon = 0.95$. The average Nusselt number decreases slightly from 6.52 for the concentric case to the minimum value 6.23 for the case of $\varepsilon = 0.75$, and then increases slightly to 6.45 for $\varepsilon = 0.95$. The plume above the top of the inner cylinder increases from one to two due to the decreased space with eccentricity. The stagnant area under the inner cylinder increases with eccentricity.

7. Conclusions

In this paper, the DQ method is employed to discretize the derivatives in the governing equations and boundary conditions to study the natural convection in a horizontal eccentric annulus between a square outer cylinder and a circular inner cylinder. The coordination transformation method is applied. The vorticity–stream function formulation is taken as the governing equation. The explicit formulation of the stream function value on the inner cylinder wall is derived from the pressure single-value condition. The DQ method is an efficient approach in computing the weak global circulation flow.

The natural convection between arbitrary eccentric cylinders for $Ra = 3 \times 10^5$ and aspect ratio of $rr = 2.6$ is systematically analyzed, including the effects of outer cylinder position on average Nusselt number, flow and thermal fields. It was found that the global circulation, flow separation and the top space between the square outer cylinder and the circular inner cylinder have significant effects on the plume inclination.

References

[1] T.H. Kuehn, R.J. Goldstein, An experimental and theoretical study of natural convection in the annulus between horizontal concentric cylinders, J. Fluid Mech. 74 (1976) 695–719.
[2] T.H. Kuehn, R.J. Goldstein, An experimental study of natural convection in the concentric and eccentric horizontal cylindrical annuli, ASME J. Heat Transfer 100 (1978) 635–640.
[3] G. Guj, F. Stella, Natural convection in horizontal eccentric annuli: numerical study, Numer. Heat Transfer 27 (1995) 89–105.
[4] R.O. Warrington, R.E. Powe, The transfer of heat by natural convection between bodies and their enclosures, Int. J. Heat Mass Transfer 28 (2) (1985) 319–330.
[5] Y. Liu, N. Phan-Thien, R. Kemp, Coupled conduction–convection problem for a cylinder in an enclosure, Comput. Mech. 18 (1996) 429–443.
[6] F. Moukalled, S. Acharya, Natural convection in the annulus between concentric horizontal circular and square cylinders, J. Thermophys. Heat Transfer 10 (3) (1996) 524–531.
[7] C.O. Ekundayo, S.D. Probert, M. Newborough, Heat transfer from a horizontal cylinder in a rectangular enclosure, Appl. Energy 61 (1998) 57–78.
[8] N.K. Ghaddar, Natural convection heat transfer between a uniformly heated cylindrical element and its rectangular enclosure, Int. J. Heat Mass Transfer 35 (10) (1992) 2327–2334.
[9] V. Deschamps, G. Desrayaud, Modeling a horizontal heat-flux cylinder as a line source, J. Thermophys. Heat Transfer 8 (1) (1994) 84–91.
[10] K. Sasaguchi, K. Kuwabara, K. Kusano, H. Kitagawa, Transient cooling of water around a cylinder in a rectangular cavity – a numerical analysis of the effect of the position of the cylinder, Int. J. Heat Mass Transfer 41 (1998) 3149–3156.
[11] R.E. Bellman, J. Casti, Differential quadrature and long-term integration, J. Math. Anal. Appl. 34 (1971) 235–238.
[12] R.E. Bellman, B.G. Kashef, J. Casti, Differential quadrature: a technique for the rapid solution of nonlinear partial differential equations, J. Comput. Phys. 10 (1972) 40–52.
[13] C. Shu, B.E. Richards, Application of generalized differential quadrature to solve two-dimension incompressible Navier–Stokes equations, Int. J. Numer. Methods Fluids 15 (1992a) 791–798.
[14] C. Shu, B.E. Richards, Parallel simulation of incompressible viscous flows by generalized differential quadrature, Comput. System Eng. 3 (1992b) 271–281.
[15] C. Shu, Y.T. Chew, Fourier expansion-based differential quadrature and its application to Helmholtz eigenvalue problems, Commun. Numer. Methods Eng. 13 (1997) 643–653.
[16] C. Shu, Differential Quadrature and its Application in Engineering, Springer-Verlag London Limited, 2000, pp. 25–38.
[17] C. Shu, H. Xue, Explicit computation of weighting coefficients in the harmonic differential quadrature, J. Sound Vib. 204 (1997) 549–555.